PHYSICAL REVIEW E

STATISTICAL PHYSICS, PLASMAS, FLUIDS, AND RELATED INTERDISCIPLINARY TOPICS

THIRD SERIES, VOLUME 61, NUMBER 6 PART B JUNE 2000

ARTICLES

Exact banded patterns from a Doi-Marrucci-Greco model of nematic liquid crystal polymers

M. Gregory Forest, Qi Wang,* and Hong Zhou

Department of Mathematics, University of North Carolina, Chapel Hill, North Carolina 27599-3250

(Received 5 March 1999; revised manuscript received 12 November 1999)

Elements of pattern formation in nematic liquid crystal polymers are presented using the Doi-Marrucci-Greco (DMG) moment-averaged theory. The theory yields a full tensor orientation equation, accounting for excluded-volume and distortional elasticity potentials, with rotational molecular diffusion. Spinodal decomposition associated with unstable homogeneous phases is described first by way of an exact solution of the linearized DMG model. A variety of uniaxial and biaxial banded spatial patterns are then explicitly constructed from the DMG model. Exact solutions are given that possess order parameter spatial variations as well as solutions whose banded intensity patterns arise from sinuous director heterogeneity. These constructions pose as analytical models for banded structures observed during and after cessation of simple shear or elongation.

PACS number(s): 61.30.−v

I. INTRODUCTION

Complex mesophases formed by anisotropic molecules have stimulated theoretical interest for many decades. The isotropic-to-nematic (*I-N*) phase transition, observed as far back as 1888 by Friedrich Reinitzer, was first explained by Onsager in 1949. Analysis based on Landau–de Gennes free energies [1–3] has been successful in predicting certain behavior of liquid crystal polymers, including aspects of phase transitions and spinodal decomposition. The kinetic and continuum theories of Hess, Doi and Edwards, Beris and Edwards, and many others [4,2,5] combines a molecular-scale description of nematic order with Landau–de Gennes free energy expressions posited at relevant length scales. These theories allow one to explain and predict how molecular-scale physics influences and dictates observed mesoscopic behavior. Furthermore, exact analysis and solutions from model equations are useful both to gain insight into observed behavior and structures and to say something about the predictability of the model itself. The analysis and exact solutions provided in this paper are so motivated.

Classical descriptions [1] of *I-N* phase transitions employ a spatially homogeneous uniaxial nematic theory. Here we focus on more general, full tensor models. Shimada, Doi, and Okano (SDO) [6] studied details of spinodal decomposition from the isotropic phase with a detailed full tensor analysis, allowing for a hard-rod interaction potential and translational molecular diffusion. They carried out a long-wave expansion near the spinodal point to predict the dominant wavelengths and orientation tensor modes of instability. Motivated by this work, we solve in closed form the linearized Doi-Marrucci-Greco (DMG) moment-averaged model to predict and compare spinodal decomposition from the unstable isotropic and unstable nematic equilibrium phases. Briefly, the physics of the SDO model versus the DMG model yields significant differences in the wavelengths and orientation modes that dominate the *I-N* transition; the DMG model predictions are consistent with a homogeneous phase transition without spatial pattern formation, whereas the SDO model reflects a finite dominant wavelength and orientation tensor (bending) mode for the unstable isotropic phase. We then show that the DMG model applied to the unstable nematic phase suggests a different scenario during spinodal decomposition: there is no preferred wavelength, yet there is a preferred orientation mode of instability.

Our main goal in this paper is to derive a hierarchy of exact liquid crystal polymer (LCP) patterns from the Doi-Marrucci-Greco [7], second-moment-averaged kinetic theory. Specifically, we describe uniaxial, spatially periodic striped or banded patterns; uniaxial traveling waves which interpolate in space and time between homogeneous equilibrium phases; and fully biaxial, irregularly banded spatial patterns. These analytical constructions arise in two distinct

*Permanent address: Department of Mathematical Sciences, Indiana University-Purdue University Indianapolis, Indianapolis, IN 46202.

ways: through order parameter oscillations with fixed directors (optical axes), and through director variations with fixed order parameters. The latter mechanism has strong experimental confirmation as the origin of shear-induced and elongation-induced banded structures [8–11].

II. DOI-MARRUCCI-GRECO THEORY

Let $\mathbf{Q}$ be the orientation tensor, a second-order, symmetric, traceless tensor that describes the average molecular orientation with respect to a probability distribution. $\mathbf{Q}$ is said to exhibit uniaxial symmetry if two of its eigenvalues are identical; otherwise, it is said to have biaxial symmetry. The orientation tensor equation in the absence of flows, in the Doi-Marrucci-Greco theory [2,7] is given by

$$\frac{d}{dt}\mathbf{Q}=-\frac{1}{\lambda}[\mathbf{F}(\mathbf{Q})+\mathbf{E}(\mathbf{Q})],$$

$$\mathbf{F}(\mathbf{Q})=(1-N/3)\mathbf{Q}-N(\mathbf{Q}\cdot\mathbf{Q})+N(\mathbf{Q}:\mathbf{Q})(\mathbf{Q}+\mathbf{I}/3), \quad (1)$$

$$\mathbf{E}(\mathbf{Q})=-\frac{Nl^2}{24}[\tfrac{1}{3}\Delta\mathbf{Q}+\tfrac{1}{2}\Delta\mathbf{Q}\cdot\mathbf{Q}+\tfrac{1}{2}\mathbf{Q}\cdot\Delta\mathbf{Q}-(\Delta\mathbf{Q}:\mathbf{Q})(\mathbf{Q}+\mathbf{I}/3)],$$

where λ is the *relaxation time* related to rotary diffusion of a rigid-rod molecule, N is the *dimensionless polymer concentration* that dictates the strength of the Maier-Saupe short-range intermolecular potential, and l is the persistence length or range of the elastic interaction.

It is customary to seek homogeneous equilibria of pure nematic theories by positing $\mathbf{Q}$ in a uniaxial representation

$$\mathbf{Q}=s_u(\mathbf{nn}-\tfrac{1}{3}\mathbf{I}), \quad (2)$$

where $\mathbf{n}$ is the distinguished unit eigenvector of $\mathbf{Q}$ corresponding to the unique simple eigenvalue (proportional to s_u); $\mathbf{n}$ is known as the uniaxial director while s_u is the uniaxial order parameter, $-\frac{1}{2}\leqslant s_u\leqslant 1$ [12]. With this ansatz, the nematodynamic equation (1) yields immediately that $\mathbf{n}$ is arbitrary and s_u is a zero of the algebraic equation

$$U(s_u)=0, \quad (3)$$

where

$$U(s_u)=s_u[1-N/3(1-s_u)(2s_u+1)] \quad (4)$$

defines the *uniaxial bulk free energy* $\int U(s)ds$, corresponding to a quartic Landau–de Gennes short-range free energy potential. The *uniaxial equilibrium branches* as functions of the concentration parameter N are given by

$$s_u^0=0, \quad s_u^{\pm}=\frac{1\pm 3\sqrt{1-8/3N}}{4}. \quad (5)$$

For quartic short-range potentials, i.e., for homogeneous tensor fields $\mathbf{F}(\mathbf{Q})$ fourth-order in $\mathbf{Q}$, all constant equilibria are uniaxial. We give a simple proof of this result for the moment-averaged Doi-Marrucci-Greco model. The result below applies to any algebraic closure approximation that preserves the order of nonlinearity in moments [13,14]; if a quintic or higher-order potential is assumed, or if a different closure rule is employed, the proof below indicates that biaxial equilibria cannot be ruled out.

Fact: All homogeneous equilibria of the DMG model (1) are uniaxial.

Proof: Since $\mathbf{Q}$ is symmetric, it can be diagonalized by an orthogonal matrix $\mathbf{P}$,

$$\mathbf{Q}=\mathbf{P}^T\mathbf{\Lambda}\mathbf{P}, \quad (6)$$

where

$$\mathbf{\Lambda}=\begin{bmatrix}\gamma_1 & & \\ & \gamma_2 & \\ & & \gamma_3\end{bmatrix}. \quad (7)$$

Substituting Eq. (6) into $F(\mathbf{Q})=0$, we have

$$\mathbf{P}^T\left[-N\mathbf{\Lambda}^2+\left(1-N/3+N\sum_{i=1}^{3}\gamma_i^2\right)\mathbf{\Lambda}+\frac{N}{3}\sum_{i=1}^{3}\gamma_i^2\mathbf{I}\right]\mathbf{P}=\mathbf{0}. \quad (8)$$

It follows that γ_1, γ_2, and γ_3 are roots of the quadratic equation

$$-Nx^2+(1-N/3+NC)x+\frac{NC}{3}=0, \quad (9)$$

where $C=\Sigma_{i=1}^{3}\gamma_i^2$. Since Eq. (9) is quadratic, it cannot have more than two distinct roots. Thus, two of the eigenvalues γ_1, γ_2, and γ_3 must be identical, which is the definition of uniaxiality.

The *dynamics* of $\mathbf{Q}$, even in a neighborhood of homogeneous uniaxial equilibria, is not necessarily uniaxial. Recall that $\mathbf{Q}$ has five independent components, e.g., in a matrix representation with respect to Cartesian coordinates,

$$\mathbf{Q}=\begin{bmatrix}Q_{11} & Q_{12} & Q_{13}\\ Q_{12} & Q_{22} & Q_{23}\\ Q_{13} & Q_{23} & -(Q_{11}+Q_{22})\end{bmatrix}. \quad (10)$$

A convenient and useful basis of symmetric, traceless, rank 2 tensors is given by [6,15]

$$\mathbf{Q}^{(1)}=\begin{bmatrix}1&0&0\\0&1&0\\0&0&-2\end{bmatrix}, \quad \mathbf{Q}^{(2)}=\begin{bmatrix}-1&0&0\\0&1&0\\0&0&0\end{bmatrix},$$

$$\mathbf{Q}^{(3)}=\begin{bmatrix}0&0&0\\0&0&1\\0&1&0\end{bmatrix}, \quad (11)$$

$$\mathbf{Q}^{(4)}=\begin{bmatrix}0&1&0\\1&0&0\\0&0&0\end{bmatrix}, \quad \mathbf{Q}^{(5)}=\begin{bmatrix}0&0&1\\0&0&0\\1&0&0\end{bmatrix}.$$

From [6], $\mathbf{Q}^{(1)}$ is a *splay mode* with respect to $\mathbf{e}_z$, $\mathbf{Q}^{(2)}$ and $\mathbf{Q}^{(4)}$ correspond to *twist modes*, and $\mathbf{Q}^{(3)}$ and $\mathbf{Q}^{(5)}$ correspond to *bend modes*. Here this fixed basis plays a funda-

mental role both in the solution of the linearized DMG system (1) about homogeneous equilibria (Sec. II A), and in deriving special classes of nonhomogeneous solutions (Sec. II B).

A. Spinodal decomposition from unstable homogeneous equilibria

The linearized stability of an arbitrary homogeneous equilibrium is determined by Fourier analysis of the constant coefficient, linearization of the tensor partial differential equation (1). For a given uniaxial equilibrium $\mathbf{Q}^*$, we set $\mathbf{Q}=\mathbf{Q}^*+\tilde{\mathbf{Q}}$, insert it into Eq. (1), and retain terms linear in $\tilde{\mathbf{Q}}$:

$$\frac{d\tilde{\mathbf{Q}}}{dt}=-\frac{1}{\lambda}\left\{\left(1-\frac{N}{3}\right)\tilde{\mathbf{Q}}-\frac{Nl^2}{72}\Delta\tilde{\mathbf{Q}}-N(\mathbf{Q}^*\cdot\tilde{\mathbf{Q}}+\tilde{\mathbf{Q}}\cdot\mathbf{Q}^*)\right.$$
$$-\frac{Nl^2}{48}(\Delta\tilde{\mathbf{Q}}\cdot\mathbf{Q}^*+\mathbf{Q}^*\cdot\Delta\tilde{\mathbf{Q}})+N(\mathbf{Q}^*:\mathbf{Q}^*)\tilde{\mathbf{Q}}$$
$$+N\left[\left(\tilde{\mathbf{Q}}+\frac{l^2}{24}\Delta\tilde{\mathbf{Q}}\right):\mathbf{Q}^*\right]\left(\mathbf{Q}^*+\frac{\mathbf{I}}{3}\right)$$
$$\left.+N(\mathbf{Q}^*:\tilde{\mathbf{Q}})\left(\mathbf{Q}^*+\frac{\mathbf{I}}{3}\right)\right\}. \tag{12}$$

Then we introduce normal modes of the form $\tilde{\mathbf{Q}}=\mathbf{Q}_0e^{\omega t+i\mathbf{k}\cdot\mathbf{x}}$, $\mathbf{Q}_0$ constant. The linearized dispersion relation (a fifth-order polynomial) for $\omega(\mathbf{k},\mathbf{Q}^*)$ follows easily. The real parts of the five roots ω_i determine the linearized stability of the associated five-dimensional dynamical system for each wave vector ($\mathbf{k}$) perturbation. One does not expect to be able to explicitly factor this fifth-degree dispersion relation nor to explicitly provide the corresponding tensorial eigenfunctions. However, we have the following remarkable result first observed by Shimada, Doi, and Okano [6] in their linearized analysis of the *I-N* transition for a different physical model.

Fact: The basis tensors $\mathbf{Q}^{(i)}$, $i=1,\ldots,5$, provide a complete set of eigenfunctions for the linearized DMG equation about arbitrary homogeneous equilibria, with corresponding growth rates ω_i listed below for each equilibrium.

1. Spinodal dynamics of the unstable isotropic phase Q=0*

All five roots of the dispersion equation, i.e., all linearized growth/decay rates, are identical, given as a function of spatial wave number by

$$\omega_i=-\frac{1}{\lambda}\left(1-\frac{N}{3}+\frac{N}{3}K^2\right),\quad i=1,\ldots,5, \tag{13}$$

where

$$K^2=\frac{\|\mathbf{k}\|^2l^2}{24} \tag{14}$$

and K is a dimensionless wave number defined with respect to the persistence length l of the elasticity potential.

We conclude that all orientation tensor eigenfunctions $\mathbf{Q}^{(i)}$ experience identical linearized behavior, so there is no distinguished orientation mode during spinodal decomposition. Further, note that the spatial dependence of the growth rates due to the Marrucci-Greco elasticity potential contributes the term $-(N/3\lambda)K^2$, analogous to diffusive regularization. Only the longest wavelengths have the potential for growth. The physical predictions from the results (13) and (14) are as follows. (1) For $0<N<3$, the isotropic phase is *stable* to all wavelength perturbations, with equal decay rates in all tensor modes. (2) For $N>3$, a finite, long-wave band of wave vector perturbations is unstable,

$$0\leqslant\|\mathbf{k}\|^2<\frac{24}{l^2}\left(1-\frac{3}{N}\right). \tag{15}$$

The *I-N* transition occurs experimentally as N increases (usually through temperature controls) slightly above the critical value $N\sim3$. The DMG model predicts that the unstable wavelengths are exceedingly long and all tensorial modes behave the same, consistent with a homogeneous *I-N* transition with no spatial structure. This is in contrast with the SDO model [6], which predicts a dominant finite wavelength of instability, with dominant growth in the bend orientation modes $\mathbf{Q}^{(3,5)}$. Thus the physics of these models leads to quite distinct spinodal decomposition from the isotropic phase, and it appears that the DMG model is consistent with the standard transition to the stable, homogeneous nematic phase.

2. The ''nematic-to-nematic'' transition: Spinodal decomposition from the unstable anisotropic equilibrium phase

Repeating the analysis for the anisotropic equilibria $s_u^{\pm}$ of Eq. (5), which exist for $N\geqslant\frac{8}{3}$, we find the explicit growth/decay rates

$$\omega_q=-\frac{1}{\lambda}[U'(s_u)+K^2(1-s_u)(2s_u+1)/3], \tag{16}$$

$$\omega_{2,4}=-\frac{1}{\lambda}\left(Ns_u+\frac{K^2}{3}(N-1)\right), \tag{17}$$

$$\omega_{3,5}=-\frac{1}{\lambda}\left[\left(1-\frac{N}{3}\right)+\frac{NK^2}{3}+\frac{1}{3}\left(\frac{K^2}{2}-1\right)Ns_u+\frac{2Ns_u^2}{3}\right], \tag{18}$$

where K is defined in Eq. (14). Note once again that the terms proportional to $-K^2$ arising from the Marrucci-Greco elasticity potential are strictly stabilizing, with $\omega_i(\mathbf{0})>\omega_i(\mathbf{k})$ for $\mathbf{k}\neq\mathbf{0}$, for all i. We easily deduce the following.

(1) The highly aligned nematic phase s_u^+ is stable for all wave vector perturbations in all tensor modes.

(2) The less aligned nematic phase s_u^- is always unstable. For $\frac{8}{3}<N<3$, s_u^- is a prolate phase, unstable to splay mode ($\mathbf{Q}^{(1)}$) perturbations ($\omega_1>0$) in an explicit wave number band $\|\mathbf{k}\|$ vs N,l; see Fig. 1. The dominant unstable wave number is $\mathbf{k}=\mathbf{0}$. For $N>3$, s_u^- is an oblate phase, unstable to twist mode ($\mathbf{Q}^{(2)},\mathbf{Q}^{(4)}$) perturbations ($\omega_2=\omega_4>0$), in an explicit band of wave numbers; see Fig. 1. The dominant unstable wave number is $\mathbf{k}=\mathbf{0}$.

This completes our analysis of spinodal decomposition for all spatially homogeneous equilibria of the DMG model

(1). We remark that uniaxial tensor analyses of stability of the oblate phase [16] yield the misleading result that s_u^- is stable for $N>3$, because the uniaxial theory allows only splay model ($\mathbf{Q}^{(1)}$) perturbations. In fact, the oblate nematic phase is never stable, and is likewise not observed experimentally unless a strong field is applied as in planar elongational flow [17,18].

With regard to physical experiments, this calculation reveals selected orientation modes in the spinodal dynamics from the unstable nematic phase (the ''nematic-to-nematic'' second-order phase transition), in contrast with the instability properties of the isotropic phase. This exact analysis, based on the physics of the DMG model, indicates that the early patterns that result from spinodal decomposition may be quite different if one first uses an applied field to stabilize an oblate nematic phase (which can be accomplished by a planar elongational flow [17,18]), followed by sudden cessation of the flow field, after which the results described here predict the subsequent spinodal decomposition. The stable, highly aligned homogeneous phase attracts all orientation modes, but with mode-dependent and wave-number-dependent decay rates. A numerical simulation of the full dynamical equations near unstable equilibria might be illuminating.

B. Heterogeneous banded patterns

We now construct the two distinct classes of banded pattern solutions, first due to order parameter variations for fixed directors, and then due to director variations for fixed order parameters. These solutions arise by positing a special form of the orientation tensor $\mathbf{Q}$.

1. Bands arising from order-parameter variations

Periodic, uniaxial patterns. The first construction is of uniaxial, periodic spatial patterns that form along an arbitrary wave vector direction $\mathbf{k}=(k_x,k_y,k_z)$. We posit

$$\mathbf{Q}=s_u(\mathbf{nn}-\tfrac{1}{3}\mathbf{I}), \quad s_u(t,\theta), \quad \theta=\sqrt{\frac{24}{l}}\mathbf{k}\cdot\mathbf{x}, \tag{19}$$

where the uniaxial director $\mathbf{n}$ is arbitrary, but constant. Note that θ is a scalar, dimensionless space variable that resolves variation in the uniaxial order parameter (s_u) along the direction $\mathbf{k}$; s_u is constant in each plane orthogonal to $\mathbf{k}$.

If we insert Eq. (19) into the DMG tensor equation (1), then a scalar nonlinear reaction-diffusion equation results for the uniaxial order parameter s_u:

$$\lambda\dot{s}_u=-U(s_u)+\frac{N}{3}h(s_u)s_u'', \tag{20}$$

where $\dot{(\ )}=(\partial/\partial t)(\ )$, and $(\ )'=(\partial/\partial\theta)(\ )$,

$$h(s_u)=(1-s_u)(2s_u+1)\geqslant 0. \tag{21}$$

All homogeneous equilibria (5) of the DMG model (1) correspond to the constant solutions of Eq. (20). Steady heterogeneous patterns are described by the nonconstant steady states of Eq. (20), which is easily manipulated to the form

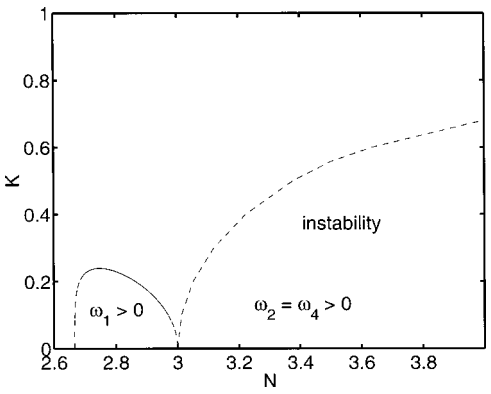

FIG. 1. Unstable wave number bands versus LCP concentration N for the nematic equilibrium phase s_u^-. The dashed curves indicate marginal stability boundaries. The less ordered nematic phase is unstable from inception, but the tensor modes of instability switch at the spinodal point $N=3$, from a splay mode long-wave instability for $\frac{8}{3}<N<3$ to a twist mode long-wave instability for all $N>3$. The persistence length is fixed arbitrarily at $l^2=24$, with the same length units used for $\mathbf{k}$, so that $K=\|\mathbf{k}\|^2$.

$$s_u''+\left[s_u+\frac{1}{N}\left(\frac{1}{s_u-1}+\frac{1}{2s_u+1}\right)\right]=0. \tag{22}$$

Equation (22) is recognized as a Hamiltonian system, with *conserved energy*

$$H(s_u,s_u')=\tfrac{1}{2}(s_u')^2+V(s_u), \tag{23}$$

and potential energy [normalized so that $V(s_u^0=0)=0$]

$$V(s_u)=\tfrac{1}{2}\left(s_u^2+\frac{1}{N}\ln[(1-s_u)^2(2s_u+1)]\right). \tag{24}$$

Figure 2 illustrates the shape of V vs N whereas Fig. 3 gives the corresponding phase portrait of Eq. (22). We note the salient features. (1) For $N<\frac{8}{3}$, V is a strictly repulsive potential and there are no bounded nonconstant solutions of Eq. (22). (2) For $\frac{8}{3}<N<3$, Fig. 2(a), the potential V develops an attractive well centered at the potential energy minimum $s_u^-\in(0,\frac{1}{4})$, leading to periodic spatial patterns that oscillate over prolate phases of s_u, Fig. 3(a), centered at s_u^-. (3) For $N>3$, V has an attractive well centered at the isotropic phase s_u^0, Fig. 2(b), leading to periodic patterns that oscillate between prolate and oblate phases, Fig. 3(b).

These periodic solutions are now translated to light scattering intensity patterns to see how they visually compare with the significant experimental documentation of *banded patterns* [8–11,19]. The range of order parameter values varies with N, while the periodic spacing of the bands depends nonlinearly on N and scales with the persistence length l. Let I be the transmitted light intensity of a light scattering experiment for an LCP material; the relative transmitted light intensity (I/I_0) is related to the normalized birefringence s_u by [20]

$$I=I_0\sin^2\left(\frac{2\pi h s_u}{\lambda_{\text{light}}}\right), \tag{25}$$

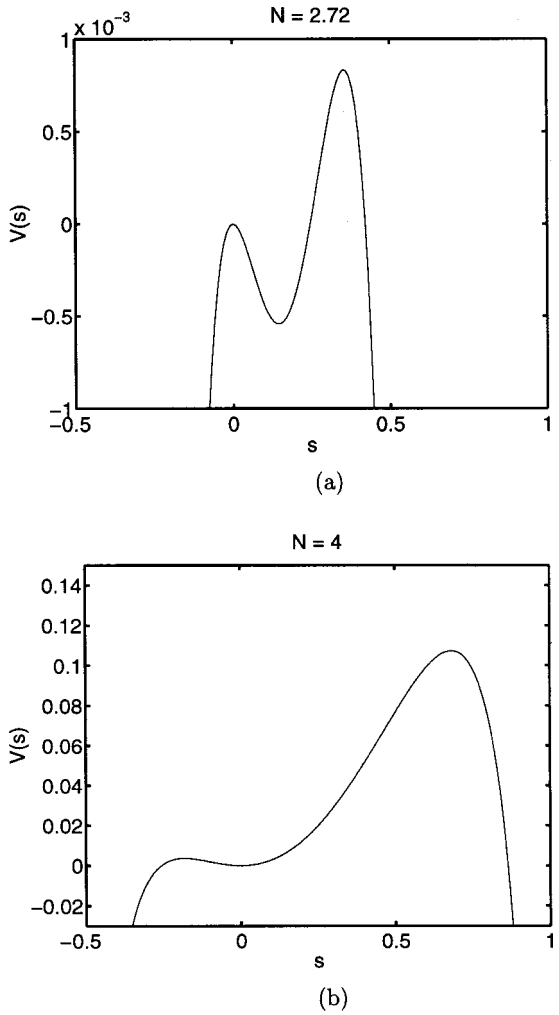

FIG. 2. Representative plots of the spatial potential energy function $V(s)$, Eq. (24), as a function of the uniaxial order parameter s, for two values of LCP concentration N: (a) $N=2.72$; (b) $N=4$.

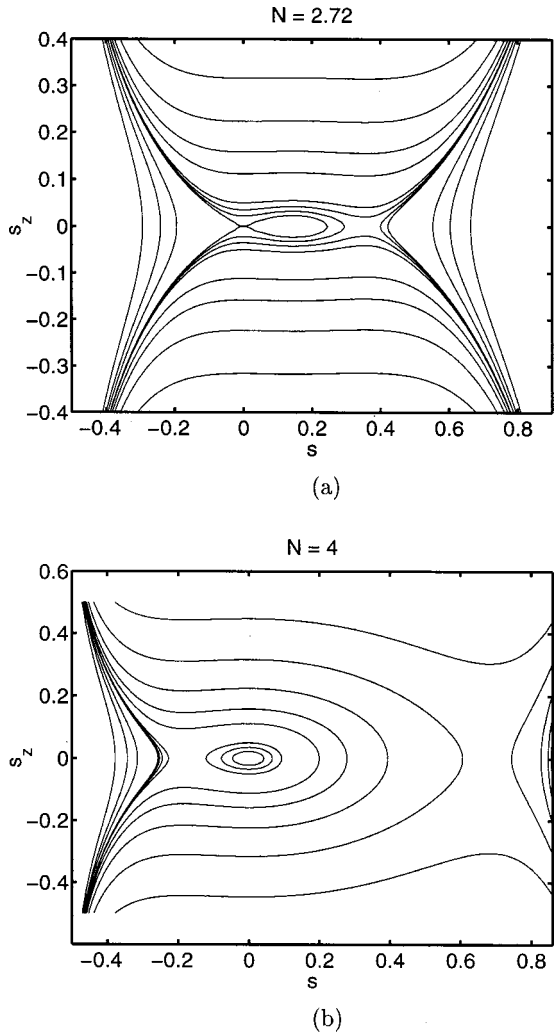

FIG. 3. The phase portrait in the phase space (s,s_z) corresponding to the potentials $V(s)$ in Fig. 2. (a) For $\frac{8}{3}<N<3$, there exist periodic patterns oscillating about the nematic phase s_u^-. (b) For $N>3$, the periodic patterns oscillate about the unstable isotropic phase s_u^0.

where h is the sample thickness and λ_{light} is the wavelength of the incident light. Figure 4 depicts the corresponding periodic pattern for a periodic solution of Figs. 2(a) and 3(a) by plotting the relative transmitted light intensity I/I_0. The parameter values used are $N=2.72$, $h=20\ \mu$m, and $\lambda_{\text{light}}=530$ nm (from [20]). At this concentration value of N, the isotropic and nematic homogeneous phases are bistable, whereas the lower-ordered nematic phase is unstable. Curiously, the patterns oscillate about the unstable nematic phase. Likewise, for $N>3$ the periodic spatial patterns oscillate about the unstable isotropic phase.

Traveling wave, uniaxial order parameter patterns. We now seek a solution of the uniaxial order parameter reaction-diffusion equation (20) in the form $s_u=s_u(Z)$, where

$$Z=\theta-ct \tag{26}$$

is a traveling wave coordinate, and c is a constant speed to be determined. This yields a ''damped nonlinear oscillator'' equation [with $(\,)'=(d/dZ)(\,)'$]

$$\frac{Nl^2}{72\lambda}(1-s_u)(2s_u+1)s_u''+cs_u'-\frac{1}{\lambda}U(s_u)=0. \tag{27}$$

The special case $c=0$ corresponds to the previous steady patterns governed by Eq. (22). For $c\neq 0$, we evaluate the directional derivative of the energy (23) along the solution of Eq. (27),

$$\frac{dH}{dZ}=\nabla H\cdot(s',s'')=-\frac{144\lambda c}{Nl^2(1-s)(2s+1)}(s')^2, \tag{28}$$

which is strictly decreasing for $c>0$ and increasing for $c<0$. Routine phase plane arguments [21] show that no periodic patterns survive for $c\neq 0$, but that infinite period, traveling waves emerge for $N>\frac{8}{3}$, which connect one equilibrium phase at $z=-\infty$ to another equilibrium phase at $z=+\infty$. Due to space limitations, we do not list all of these isotropic-to-nematic and nematic-to-nematic traveling waves, but suffice it to say that for each potential energy shape depicted in Fig. 3 there is a solution that connects each pair of equilibria [21].

Because of the complicated nonlinearity of Eq. (27), we cannot produce a closed-form, recognizable expression for these traveling waves. Representative solutions can be calcu-

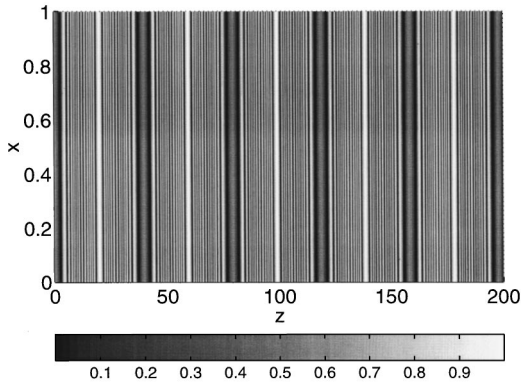

FIG. 4. A representative uniaxial, spatially periodic pattern corresponding to a periodic solution from Figs. 2(a) and 3(a) with $N=2.72$ and energy $H(s)$ between $H(s_u^-)$ and $H(s_u^0)$. The band or stripe pattern represents the relative transmitted light intensity, Eq. (25), calculated from the periodic order parameter solution.

lated numerically by a shooting method. An exemplary isotropic-to-nematic traveling wave is given in Fig. 5 for $N=4$.

Heterogeneous biaxial order parameter patterns. It is straightforward to lift the previous uniaxial construction to allow for both order parameters to vary along the wave vector direction **k**. For simplicity we fix the directors along the coordinate axes and posit a biaxial form of **Q**:

$$\mathbf{Q}=s(\mathbf{e}_z\mathbf{e}_z-\tfrac{1}{3}\mathbf{I})+\beta(\mathbf{e}_y\mathbf{e}_y-\tfrac{1}{3}\mathbf{I}), \tag{29}$$

and suppose the order parameters s,β depend only on (t,θ), where $\theta=\mathbf{k}\cdot\mathbf{x}$. Then the DMG model (1) reduces to a pair of one-space-dimensional (θ), coupled reaction-diffusion equations for s and β [with $(\,)'=(\partial/\partial\theta)(\,)$]:

$$\begin{aligned} s_t=&-\frac{1}{\lambda}\left[U(s)+\frac{2Ns\beta}{3}(1-s+\beta)\right]+\frac{Nl^2}{72\lambda}[(1+s-\beta\\ &+s\beta-2s^2)s''+s(s-2\beta-1)\beta''], \end{aligned} \tag{30}$$

$$\begin{aligned} \beta_t=&-\frac{1}{\lambda}\left[U(\beta)+\frac{2Ns\beta}{3}(1+s-\beta)\right]\\ &+\frac{Nl^2}{72\lambda}[\beta(\beta-2s-1)s''+(1+\beta-s+s\beta-2\beta^2)\beta'']. \end{aligned}$$

Moreover, steady biaxial patterns are given by solutions of the coupled second-order ordinary differential equations (ODEs) for s,β:

$$\begin{aligned} s''=&-\frac{24}{l^2}\left[s+\frac{1}{N}\left(\frac{1}{s+\beta-1}+\frac{1}{2s+1-\beta}\right)\right],\\ \beta''=&-\frac{24}{l^2}\left[\beta+\frac{1}{N}\left(\frac{1}{s+\beta-1}+\frac{1}{2\beta+1-s}\right)\right]. \end{aligned} \tag{31}$$

Note that the uniaxial periodic patterns of Sec. II B 1 are recovered in the uniaxial limits $(s=s_u,\beta=0)$, $(s=0,\beta=s_u)$, and $s=\beta=-s_u$. All physical biaxial patterns of Eq. (31) must have (s,β) values that lie inside the triangular region illustrated in Fig. 6; this domain is a consequence of standard eigenvalue inequalities. The tensor $\mathbf{M}=\mathbf{Q}+\frac{1}{3}\mathbf{I}$, has identical eigenvectors $\mathbf{n}_i$ as **Q**, but eigenvalues $0\leqslant d_i\leqslant 1$, $\Sigma_{i=1}^3 d_i=1$. The order parameters s,β are related to d_i by

$$s=d_3-d_1,\quad \beta=d_2-d_1. \tag{32}$$

Note that the rational terms in Eq. (31) become infinite along the boundaries of the triangle, analogous to the behavior of the uniaxial equation (22) at the order parameter bounds $-\frac{1}{2}$ and 1, which preserve solutions inside the triangle.

Observe that in the limit of $N\to\infty$, these equations (31) limit to uncoupled identical harmonic oscillators. This suggests that for N large and finite, oscillatory patterns will survive. In Fig. 6 we give a numerical biaxial pattern solution for $N=8$, which has a rich spatial oscillatory behavior. Figure 7 depicts the corresponding biaxial patterns by plotting the relative transmitted intensity functions I_{ij}/I_0 in the $\mathbf{n}_i$-$\mathbf{n}_j$ plane, which are defined in Eq. (25) with s_u replaced by d_i-d_j $(i,j=1,\ldots,3,\ i\neq j)$:

$$I=I_0\sin^2\left[\frac{2\pi h(d_i-d_j)}{\lambda_{\text{light}}}\right]. \tag{33}$$

Note that two independent planar measurements are necessary to resolve a fully biaxial pattern.

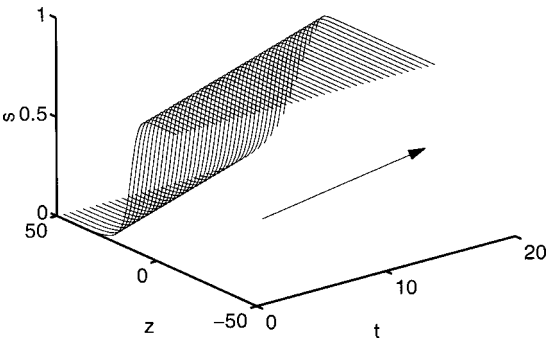

FIG. 5. A traveling wave solution connecting the homogeneous isotropic equilibrium $s_u^0=0$ and the highly aligned anisotropic homogeneous equilibrium $s_u^+=0.6830$ for LCP concentration value $N=4$. The wave speed is $c=2$.

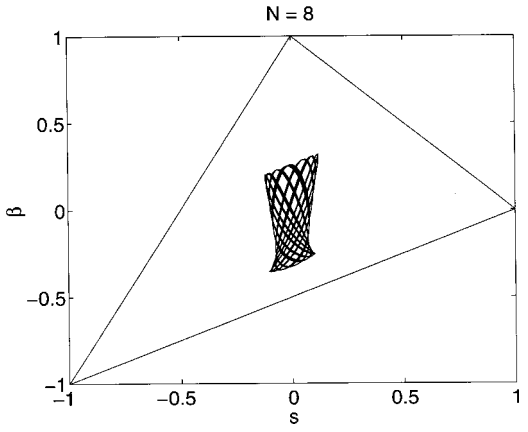

FIG. 6. Fully biaxial, steady oscillatory solutions of system (31) for LCP concentration parameter $N=8$.

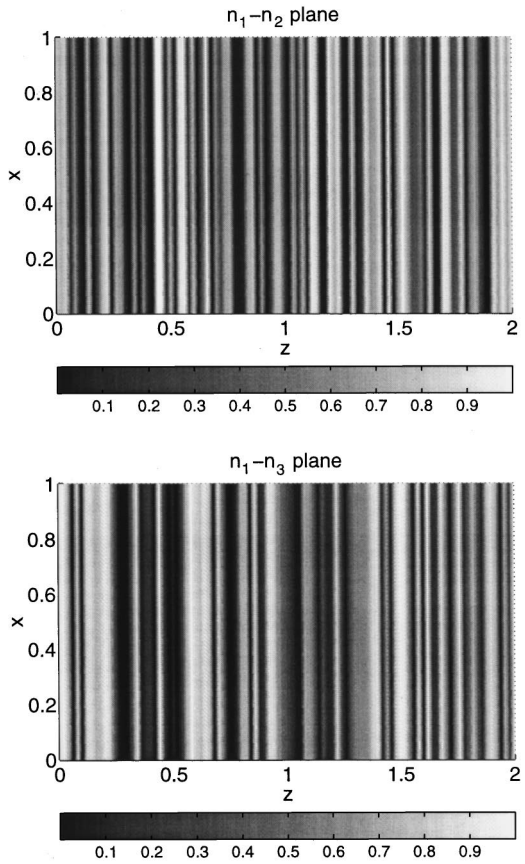

FIG. 7. Banded intensity patterns in two planar projections constructed from the biaxial order parameter solution of Fig. 6. Because the solution is fully biaxial, the intensity patterns are different in each planar projection.

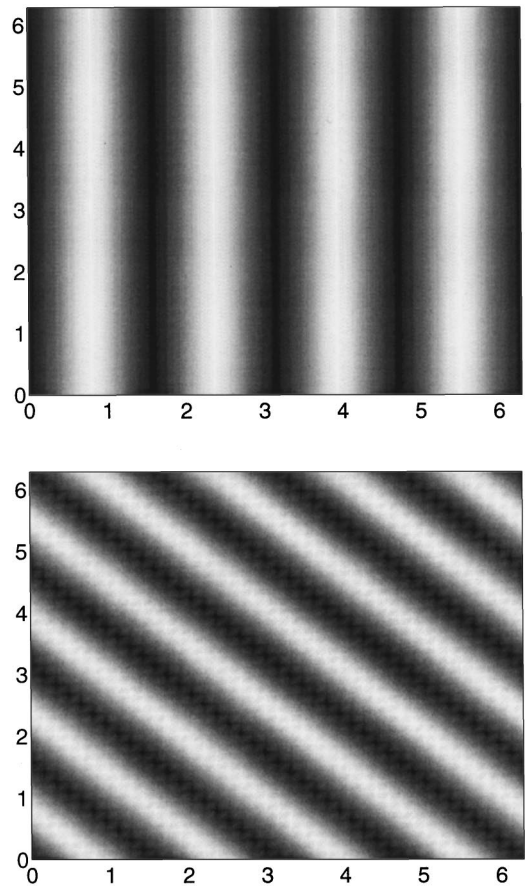

FIG. 8. Banded intensity patterns due to sinuous optical axes, characterized by Eqs. (34)–(38). Top: wave vector $\mathbf{\Gamma}=(1,0,0)$. Bottom: wave vector $\mathbf{\Gamma}=(1,1,0)$.

2. Banded biaxial patterns due to sinuous optical axes

We now construct banded patterns corresponding to fixed order parameters and sinuous optical axes. These director-induced structures are consistent with experiments that show that bright and dark light scattering regions can be interchanged by rotation of samples [22,10].

This family of exact solutions of the DMG theory is captured by the following orientation tensor form, where we fix one director ($\mathbf{e}_z$) and allow variation of the director pair in the x-y plane:

$$\mathbf{Q}=s(t)\left(\mathbf{n}(x,y,z)\mathbf{n}(x,y,z)-\frac{\mathbf{I}}{3}\right)+\beta(t)\left(\mathbf{e}_z\mathbf{e}_z-\frac{\mathbf{I}}{3}\right). \tag{34}$$

The ansatz (34) yields exact solutions if we choose the optical axes $\mathbf{n},\mathbf{m},\mathbf{e}_z$ to satisfy

$$\Delta\mathbf{n}=-\gamma^2\mathbf{n},\quad \gamma^2=\gamma_1^2+\gamma_2^2+\gamma_3^2,$$
$$\nabla\cdot\mathbf{n}=\mathbf{\Gamma}\cdot\mathbf{m},\quad \mathbf{\Gamma}=(\gamma_1,\gamma_2,\gamma_3), \tag{35}$$

which then leaves a coupled ODE system for the order parameters (s,β):

$$s_t=-\frac{1}{\lambda}\left(U(s)+\frac{2N}{3}s\beta(1+\beta-s)+\frac{4Nl^2\gamma^2}{3}s(1-\beta)\right),$$
$$\beta_t=-\frac{1}{\lambda}\left(U(\beta)+\frac{2N}{3}s\beta(1-\beta+s)+\frac{2Nl^2\gamma^2}{3}\times s(1-\beta-3s\beta)\right). \tag{36}$$

Solutions of these coupled harmonic equations (35) for $\mathbf{n}$ and $\mathbf{m}$ are given by

$$\mathbf{n}=(\cos(\mathbf{\Gamma}\cdot\mathbf{x}+\theta_0),\sin(\mathbf{\Gamma}\cdot\mathbf{x}+\theta_0),0), \tag{37}$$

$$\mathbf{m}=(-\sin(\mathbf{\Gamma}\cdot\mathbf{x}+\theta_0),\cos(\mathbf{\Gamma}\cdot\mathbf{x}+\theta_0),0), \tag{38}$$

where $\mathbf{x}=(x,y,z)$, θ_0 is an arbitrary constant, and $\mathbf{\Gamma}$ is the spatial wave vector.

In each plane $(x,y,z)\cdot\mathbf{\Gamma}=\text{const}$ and the orientation tensor $\mathbf{Q}$ is identically constant; all variation in $\mathbf{Q}$ takes place along the normals given by the wave vector $\mathbf{\Gamma}$. Along this direction, the degrees of orientation are fixed by constant equilibria of the s,β ODEs (36), while the optical axes $\mathbf{n}$ and $\mathbf{m}$ exhibit sinuous variations. Note that the order parameter equilibria (s^*,β^*) are biaxial because of the perturbative quadratic terms in s,β proportional to $l^2\gamma^2$. Thus the homogeneous degrees of orientation are coupled to the wave vector $\mathbf{\Gamma}$ of the sinuous optical axes.

Equation (36) has nontrivial biaxial solutions ($s\neq 0$) only if γl is relatively small, which injects an intriguing link be-

tween the previously arbitrary wave vector $\mathbf{\Gamma}$ and the persistence length l of the distortional elasticity potential.

Figure 8 depicts the intensity pattern, using the relation (33), for the same parameters as Figs. 6 and 7, with two different choices of the wave vector $\mathbf{\Gamma}$. The relation of the wave vector to the optical axes determines the structure of the intensity pattern. Note that the degrees of orientation are picked by the concentration and strength of the two potentials, leaving the optical axes and wave vector direction free to another selection mechanism, which we surmise to be the orientation of the imposed flow.

III. CONCLUSION

We have analyzed basic elements of pattern formation in liquid crystal polymers by the Doi-Marrucci-Greco, moment-averaged theory. We begin with a complete linearized analysis of all homogeneous equilibrium phases. The physics of the DMG model indicates a long-wave instability transition from both the unstable isotropic and unstable nematic equilibria; thus there is no preference toward spatial pattern structure during these phase transitions. The sole distinction between the linearized behavior of the isotropic vs the nematic phase is that the isotropic phase experiences instability in all orientation tensor modes, whereas the nematic phase has instability only in specific tensor modes (splay at low concentrations $\frac{8}{3}<N<3$, then switching over to twist modes above $N=3$).

The main focus of the paper is the explicit construction of a variety of heterogeneous spatial patterns: uniaxial periodic banded structures; traveling wave uniaxial patterns; and fully biaxial, irregularly banded patterns. These spatial structures are natural equilibria of the DMG model that exist in the balance between excluded-volume and Marrucci-Greco elasticity potentials. These exact solutions of the DMG model arise in two distinct physical realizations: either from order parameter variations with fixed optical axes, or through sinuous optical axes with homogeneous order parameters. Light intensity patterns reconstructed from these solutions are reminiscent of banded structures observed during and after cessation of simple shear and elongation flows [8–11,19], though the experimental evidence strongly suggests the sinuous optical axis origin of bands. The analytical results contained here suggest that such structures may have their origins in the pure nematic interplay between short-range excluded-volume effects and intermediate-range distortional elasticity; in this scenario applied flow fields then select, as opposed to create, the observed patterns. The role of these or analogous exact solutions would be worth pursuing both as a guide for understanding mesoscale pattern selection and as a benchmark for the application of the DMG model.

ACKNOWLEDGMENT

This effort was sponsored by the Air Force Office of Scientific Research, Air Force Materials Command, USAF, under Grant Nos. F49620-97-1-0001 and F49620-99-1-0003.

[1] P. G. de Gennes, *The Physics of Liquid Crystals* (Clarendon, London, 1974).
[2] M. Doi and S. F. Edwards, *The Theory of Polymer Dynamics* (Clarendon, London, 1986).
[3] A. Grosberg and A. Khokhlov, *Statistical Physics of Macromolecules* (AIP, New York, 1994).
[4] A. N. Beris and B. J. Edwards, *Thermodynamics of Flowing Systems with Internal Microstructures* (Oxford University Press, New York, 1994).
[5] S. Hess, Z. Naturforsch. A **31**, 1034 (1976).
[6] T. Shimada, M. Doi, and K. Okano, J. Chem. Phys. **88**, 7181 (1988).
[7] G. Marrucci and F. Greco, Mol. Cryst. Liq. Cryst. **206**, 17 (1991).
[8] A. M. Donald and A. H. Windle, *Liquid Crystalline Polymers* (Cambridge University Press, Cambridge, 1992).
[9] R. G. Larson, *The Structure and Rheology of Complex Fluids* (Oxford University Press, London, 1999).
[10] C. Viney, A. M. Donald, and A. H. Windle, J. Mater. Sci. **18**, 1136 (1983).
[11] C. Viney, A. M. Donald, and A. H. Windle, Polymer **26**, 870 (1985).
[12] M. G. Forest, Q. Wang, and S. Bechtel, Physica D **99**, 527 (1997).
[13] E. J. Hinch and L. G. Leal, J. Fluid Mech. **76**, 187 (1976).
[14] Q. Wang, J. Non-Newtonian Fluid Mech. **72**, 141 (1997).
[15] A. Sonnet, A. Killian, and A. Hess, Phys. Rev. E **52**, 718 (1995).
[16] See H. M. Doi and R. G. Larson, J. Chem. Phys. **92**, 792 (1990).
[17] M. G. Forest, Q. Wang, and H. Zhou, Phys. Fluids **12**, 490 (2000).
[18] A. Rey, Macromol. Theory Simul. **4**, 857 (1995).
[19] J. Hou *et al.*, Polymer **35**, 699 (1994).
[20] P. T. Mather, A. Romo-Uribe, C. D. Han, and S. S. Kim, Macromolecules **30**, 7977 (1997).
[21] J. Smoller, *Shock Waves and Reaction-diffusion Equations* (Springer-Verlag, New York, 1994).
[22] P. Mather, W. Burghardt, and A. Rey (private communications).